ISSN 2278-3091
Volume 9, No.1.4, 2020
International Journal of Advanced Trends in Computer Science and Engineering
Available Online at http://www.warse.org/IJATCSE/static/pdf/file/ijatcse0491.42020.pdf
https://doi.org/10.30534/ijatcse/2020/0491.42020

A Modified Chan-Vese Active Contour for Iris Segmentation on Non-Ideal and Noisy Iris

Shahrizan Jamaludin[1,2,3*], Nasharuddin Zainal[4]
[1]Department of Maritime Technology, Faculty of Ocean Engineering Technology and Informatics, Universiti Malaysia Terengganu, Malaysia, shahrizanj@umt.edu.my
[2]Renewable Energy and Power Research Interest Group (REPRIG), Eastern Corridor Renewable Energy Special Interest Group, Faculty of Ocean Engineering Technology and Informatics, Universiti Malaysia Terengganu, Malaysia, shahrizanj@umt.edu.my
[3]Marine Materials Research Interest Group, Faculty of Ocean Engineering Technology and Informatics, Universiti Malaysia Terengganu, Malaysia, shahrizanj@umt.edu.my
[4]Department of Electrical, Electronic and Systems Engineering, Faculty of Engineering and Built Environment, Universiti Kebangsaan Malaysia, Malaysia, nasharuddin.zainal@ukm.edu.my

ABSTRACT

Iris recognition has become a prominence feature in biometric system. The main advantages of iris recognition are high accuracy, high speed and easy to use. However, the non-ideal and noisy iris can contribute to a low recognition accuracy of iris recognition. Non-ideal iris is a condition where the shape of iris is not symmetrical. Meanwhile, noisy iris is a low quality iris image due to the interference of eyelashes, eyelids, specular reflections, corneal reflections and many more. Moreover, the current Chan-Vese active contour methods have shortcoming to determine the accurate initial contour. Hence, this paper presents a modified Chan-Vese active contour for iris segmentation on non-ideal and noisy iris. In this study, the Chan-Vese active contour is modified by introducing a new equation to segment both non-ideal and noisy iris simultaneously. The proposed method is also developed to improve the segmentation accuracy, recognition accuracy and image quality of iris segmentation. Next, the proposed method is compared with the other Chan-Vese active contour iris segmentation methods. According to the results, the proposed method can achieve the better performance than the other methods in terms of segmentation accuracy (97%), recognition accuracy (0.9729) and image quality (0.9915). The results show that the proposed method is efficient to segment both non-ideal and noisy iris.

Key words : Iris recognition; non-ideal; noisy iris; modified Chan-Vese active contour; iris segmentation.

1. INTRODUCTION

Iris recognition is a biometric system focuses on the iris pattern of human iris. It uses rich features of iris pattern to identify and verify the identity of human. This biometric system has become a prominent feature in pattern recognition field due to its high accuracy [1], [2], high speed [3] and easy to use [4] characteristics. However, the performance of iris recognition can be affected because of the internal and external interferences. Two main shortcomings in iris recognition are the non-ideal and noisy iris. Non-ideal iris is a situation where the shape of iris is not symmetrical. Iris is not a circular object in human eyes due to the occlusion by eyelids and eyelashes [5]. Other than that, the angular during iris acquisition may also contribute to the non-ideal iris. Meanwhile, noisy iris is a low quality iris image due to the interference of specular reflections, corneal reflections, noises, eye rotation, motion blur, off-angle and many more. The movement of camera and subject during iris acquisition might also contribute to the noisy iris. Moreover, iris acquisition with near infra-red (NIR) and visible wavelength (VW) sources can contribute to different noises. Iris images acquired with NIR may produce specular reflections, corneal reflections, non-uniform intensity, and low illumination level from the lighting sources. Meanwhile, iris images acquired with VW can be interfered by speckle, Poisson, and Gaussian noises.

Previously, the Chan-Vese active contour was used to overcome the shortcomings in non-ideal iris [6]. This method used pixel property method to localize pupillary boundary, while Chan-Vese active contour was used to localize limbic boundary as shown in Figure 1. The pixel property method detected the correct pupillary boundary based on the given threshold. In the other hand, the correct limbic boundary was detected because of the accurate position of initial contour. The advantage of this method is it managed to locate the accurate boundaries in the non-ideal iris. However, the given threshold might not accurate if implemented on a different iris database. Meanwhile, the geodesic active contour was used to segment iris region in non-ideal iris [7]. For

pre-processing, Otsu multilevel thresholding was used to delimit iris region. After that, geodesic active contour with novel stopping function was introduced to segment accurate iris region. The advantage of this method is it managed to stop evolution of active contour to segment the accurate iris region. Unfortunately, the geodesic active contour required more execution time than the Chan-Vese active contour. Moreover, the geodesic active contour depended on edges or gradient information which may cause problems if implemented on a weak iris boundary.

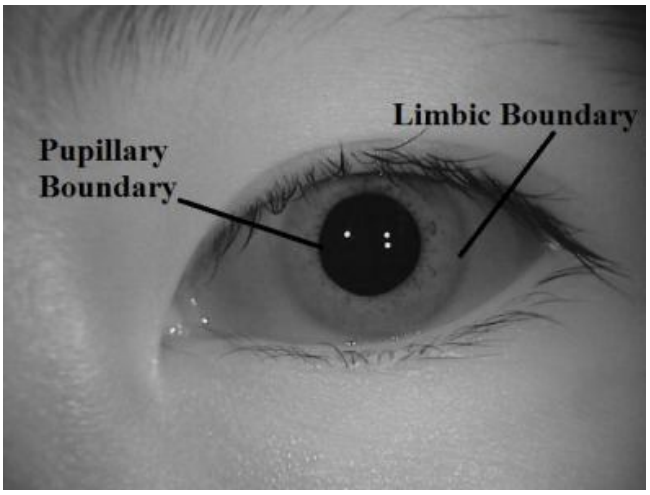

Figure 1: Pupillary and Limbic Boundaries

An improved Chan-Vese active contour was used to overcome noisy iris in [2]. The proposed method used an improved position of initial contour to localize the accurate iris boundary. This method managed to localize both pupillary and limbic boundaries, even with the presence of noises such as occlusion and specular reflection. However, the result might be different if implemented on a different database due to the assigned threshold value. Moreover, this method focused on the partial iris segmentation instead of the full iris segmentation. Meanwhile, the Histogram of Oriented Gradients (HOG) and Support Vector Machine (SVM) were used for automated iris segmentation in an unconstrained environment [8]. The HOG was used for iris structure description, while SVM was used for iris classification. This method was efficient due to its ability to segment iris region with noise, eye rotation, motion blur and off-angle, in a visible wavelength environment. Unfortunately, this method required pre-processing which can degrade the quality of iris features.

Due to the shortcomings in previous methods, this paper presents a modified Chan-Vese active contour for iris segmentation on non-ideal and noisy iris. In this study, the Chan-Vese active contour is modified by introducing a new equation to segment both non-ideal and noisy iris simultaneously. The proposed method is also developed to improve the segmentation accuracy, recognition accuracy and image quality of iris segmentation. Two contributions are achieved in this study: (a) segmenting non-ideal shape of pupillary and limbic boundaries in non-ideal iris; (b) segmenting iris region with the presence of noise such as eyelids and eyelashes occlusions, and non-uniform intensity in noisy iris.

2. MATERIALS AND METHODS

The proposed method involves pupillary boundary segmentation, initial contour, limbic boundary segmentation, normalization, feature extraction and matching. Descriptions of the proposed method are given in the following subsections.

2.1 Pupillary Boundary Segmentation

Pupillary boundary segmentation is easier due to a high contrast between pupil and iris region. In [6], pupillary boundary was segmented with pixel property method. Specular reflections were eliminated before the detected pupil region was filled with morphological closing. After that, pupillary boundary was segmented from the area and pixel list of the detected pupil region.

In this paper, the pixel property method is exploited because of its efficiency. Due to that, a modification of this method is proposed to improve pupillary boundary segmentation. Firstly, pixel property method is applied to calculate number of interconnecting regions in iris image. After that, all information regarding area and pixel list of the interconnecting regions is stored in a list. Then, the largest region from the list is chosen as a pupil region and the pupillary boundary can be segmented accordingly. The proposed method is different than [6] since specular reflections are not eliminated from the pupillary boundary. This is because the pupillary boundary segmentation is less dependent on the presence of specular reflections due to a huge contrast difference between them. Hence, the method to eliminate specular reflections is excluded from the proposed method.

2.2 Initial Contour

Initial contour is an important element in the Snake [9], Geodesic [10] and Chan-Vese [11] active contours. The purpose of initial contour is to determine the starting process of segmentation. Active contour will start converging inside or outside of the desired boundary from the initialization of initial contour. Initialization of initial contour is important to avoid segmenting a separate boundary [12].

However, initial contour is the main problem in active contour since the level set function must sign distance to initial contour. Moreover, initialization of initial contour may be fraught with the problems of how and where to assign the

initial contour [13]–[16]. Different size and position of initial contours on the same image can produce different results. Other than that, the iteration number is totally dependent on the initial contour size and position. A large iteration number is needed for the level set function to come to a steady state [13]. So far, this is a great challenge in active contour and no simple answer applies for initialization problem.

Hence in this study, an efficient way to tackle initialization problem is proposed. A circle function as in (1) is used for initialization of initial contour as in [2] and [6], where *r* is the radius of circle and *x, y* is the center point coordinate of circle.

$$c = r - \sqrt{(x-a)^2 + (y-b)^2} \tag{1}$$

The circle function is used because of the shape of iris is almost circular or oval. However, since the shape of iris is not symmetrical and varied upon off-angle and eye rotation, a new parameter $3.5r_p$ is proposed into the existing circle function as in (2), where:

$$c = 3.5r_p - \sqrt{(x-x_c)^2 + (y-y_c+k)^2} \tag{2}$$

r_p is the radius of pupil, x_c, y_c is the center point coordinate of pupil, and *k* is the shifted y-axis. The value of 3.5 is added to accommodate limbic boundary into the initial contour. This value is chosen since the average size of iris is within 3.5 times of pupil region. In the other hand, the parameter of *k* obtained from [2] is also added into the circle function in order to avoid the rich texture of upper eyelid that might affect the segmentation accuracy. The upper eyelid has a lot of energy levels and rich edges which are difficult to segment by an ordinary segmentation method [2]. Finally, the proposed circle function is assigned as an initial contour of the Chan-Vese active contour which will be used in the next subsection to segment limbic boundary. The example of initial contour is shown in Figure 2.

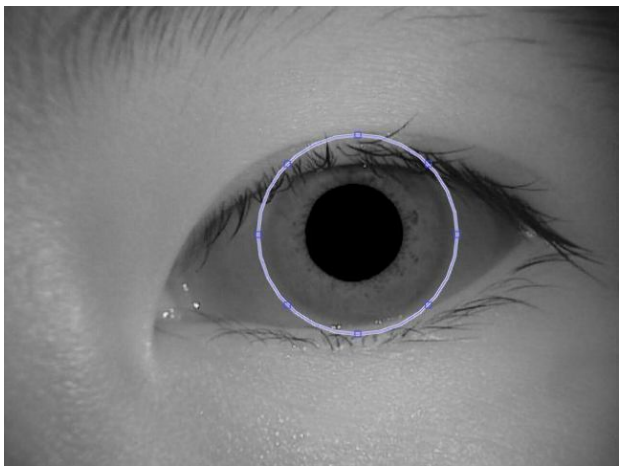

Figure 2: Initial Contour

2.3 Limbic Boundary Segmentation

Next, the proposed initial contour, *c* is applied to the Chan-Vese active contour, *F* as in (3):

$$\begin{aligned} F(c_1, c_2, C) = {} & \mu \cdot Length(C) + v \cdot Area(inside(C)) \\ & + \lambda_1 \int_{inside(C)} |\mu_0(x,y) - c_1|^2 \, dxdy \\ & + \lambda_2 \int_{inside(C)} |\mu_0(x,y) - c_2|^2 \, dxdy \end{aligned} \tag{3}$$

where Length is the length of curve C, Area is the area of curve C, $\mu = \upsilon \geq 0$, fit weight λ_1 is the force inside C, λ_2 is the force outside C where $\lambda_1 = \lambda_2 = 1$, μ_0 (x, y) is the input image [2], [11]. F is minimized by adding functions of C and area of C, inside and outside of iris image [5]. The regularity by penalizing the length of C is represented in the first term of the equation (smooth factor, μ), while the size of C is controlled in the second term (contraction bias, υ) [6]. For further explanation of the Chan-Vese active contour, we refer our readers to [11]. The values of smooth factor ≤ 1.5, contraction bias ≤ 0.7 and iteration number ≤ 35 are assigned to the Chan-Vese active contour which are obtained from [2].

Next, the Chan-Vese active contour with the proposed initial contour and parameters is implemented on the iris image. The respective active contour will start segmentation process from the initial contour, and then will converge inwards to determine the accurate limbic boundary. The Chan-Vese active contour will stop converging when it reaches a steady state in the iris image.

2.4 Normalization, Feature Extraction and Matching

After iris image is segmented with the modified Chan-Vese active contour, then normalization is applied to convert the segmented iris into a rectangular coordinate. The used normalization method is based on the Rubber sheet model as in [17], [18]. However, the algorithm is modified to improve its efficiency during the normalization process. The GPU arrays are used to store temporary data, hence can reduce execution time by two folds as in [2]. The example of normalization is shown in Figure 3.

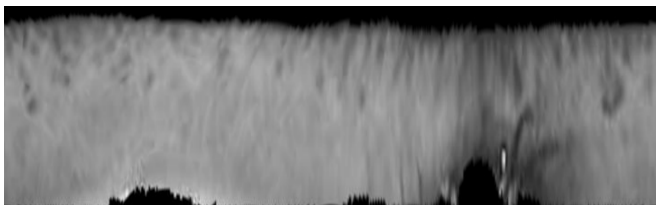

Figure 3: Normalization with the Rubber Sheet Model

Then, the rich texture of iris pattern is extracted with 2D Gabor filter as shown in Figure 4. The data from iris are encoded into a binary data to create an iris template. The

created iris template will be matched with the database template to determine matching score. Matching method used here is similar with the Hamming distance as in [19]–[23]. However, this method is improved with GPU arrays as in normalization method [24], [25].

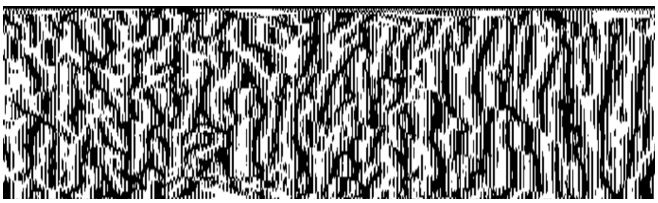

Figure 4: Feature Extraction with 2D Gabor Filter

3. RESULTS AND DISCUSSION

This section is represented in two subsections: (a) Performance Evaluation will describe metrics used to measure performance of the proposed method; (b) Experimental Result will explain and discuss findings from the experiment.

3.1 Performance Evaluation

This subsection describes the evaluation metrics used to measure performance of the proposed method. The individual segmentation accuracy, SA_K is calculated from (4) where: r x c is the resolution of iris image I and ground truth image G. Both images XORed together to determine number of pixels that hits each other, which produces similarity score.

$$SA_k = \frac{1}{r \times c} \sum_{i=1}^{r} \sum_{j=1}^{c} \left(I_{i,j} \otimes G_{i,j} \right) \tag{4}$$

After that, the average value of all individual iris images is calculated as in (5), to obtain the overall segmentation accuracy, SA where N is the total number of iris images.

$$SA = \frac{1}{N} \sum_{k=1}^{N} SA_k \tag{5}$$

For recognition accuracy, the receiver operating characteristic (ROC) curve is obtained by plotting the false acceptance rate (FAR) against the genuine acceptance rate (GAR). The GAR is obtained from 1 – FRR, where FRR is the false acceptance rate. Both FAR and FRR are obtained from the matching scores as in subsection 2.4. After that, the area under curve (AUC) is calculated from the ROC curve which represents the recognition accuracy of the respective methods.

For evaluation of image quality, the structural similarity index (SSIM) is used as shown in (6) where: x is the original image, y is the processed image, μ_x is the average x, μ_y is the average y, σ_{xy} is the covariance of x and y, σ_{2x} is the variance of x and σ_{2y} is the variance of y.

$$SSIM(x, y) = \frac{(2\mu_x\mu_y + c_1)(2\sigma_{xy} + c_2)}{(\mu_x^2 + \mu_y^2 + c_1)(\sigma_x^2 + \sigma_y^2 + c_2)} \tag{6}$$

This method measures image degradation of two iris images caused by transmission lost, image compression and image restoration. The SSIM estimates image degradation of a processed image from a reference image by perceiving changes. In iris recognition, SSIM is used to calculate quality of iris images after the iris segmentation process. This is to determine if the rich texture of iris pattern is changed during iris segmentation. The less changed iris image will record a score of 1. However, this method only measures the perceptual difference between both iris images (before and after iris segmentation process). The SSIM cannot judge which of the two iris images is better, which can only be known from the original iris image.

3.2 Experimental Result

The experiments are conducted on a computer with Intel Core i5 2.3 GHz processor, 4 GB RAM memory and Matlab software. According to Figure 5, the proposed method managed to segment the accurate pupillary and limbic boundaries. This happened because of the non-ideal and noisy pupillary and limbic boundary were successfully segmented by the proposed method as stated in Section 2. The pixel property method was used to segment the non-ideal pupillary boundary. However, this method was modified from [6], where a method to eliminate specular reflections was excluded to reduce complexity during segmentation process. The proposed method not only can segment the non-ideal pupillary boundary, but also the noisy pupillary region even after the specular reflection method was excluded from the algorithm. This showed that the proposed method can simultaneously segment the non-ideal and noisy pupillary boundary.

Besides that, the non-ideal and noisy limbic boundary was also successfully segmented by the modified Chan-Vese active contour. The initialization of initial contour was a success, thus the non-ideal and noisy limbic boundary managed to be segmented simultaneously. The problems of how and where to assign initial contour were solved by introducing the modified circle function as in subsection 2.2. Other than that, the iteration number needed for the level set function to come to a steady state was reduced to minimum by using the modified circle function.

In terms of segmentation accuracy, the proposed method achieved the highest accuracy (97%) compared to [2] (45%) and [6] (95%). This happened because of the proposed method had the better initialization of initial contour than [2] and [6]. The proposed initial contour was based on the modified circle function, where the size and position were more accurate than the initial contours in [2] and [6].

Moreover, the proposed method used minimum iteration number than the other methods. Method in [2] achieved the lowest segmentation accuracy because of it focused on the lower part of iris region only. This method called sub-iris technique where it segmented the rich texture of iris pattern near to the pupillary boundary.

In terms of recognition accuracy, the proposed method achieved a high recognition accuracy (0.9729) than [6] (0.9701). This happened because of the proposed method recorded a bigger AUC than [6]. This showed that a high segmentation accuracy can produce a high recognition accuracy if implemented on the full iris region. However, the proposed method was less accurate than [2]. This happened since [2] focused on the rich texture of iris pattern near to the pupillary boundary only. Hence, this comparison was not adequate since the proposed method focused on the full iris region instead of on the selected part of iris region.

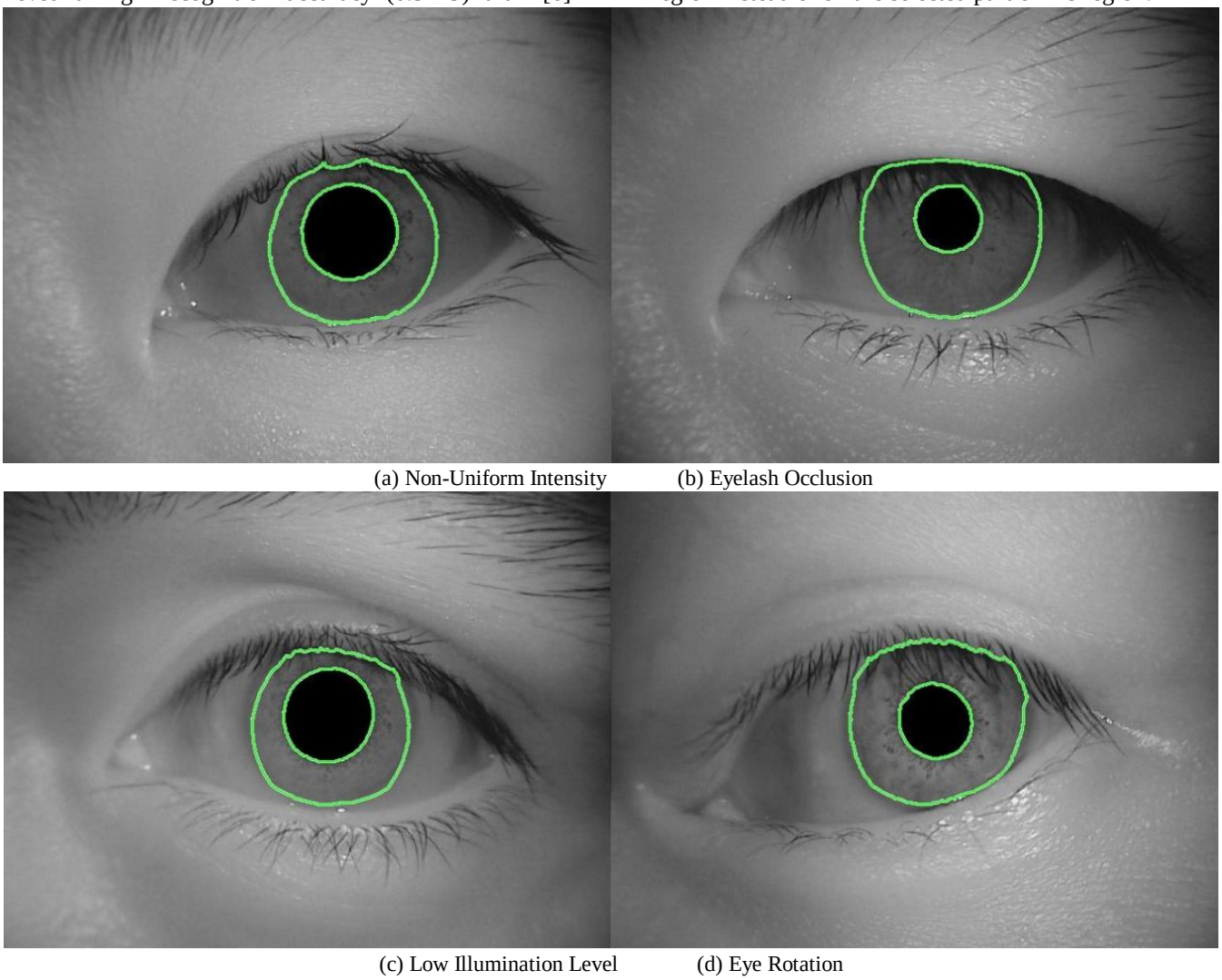

(a) Non-Uniform Intensity (b) Eyelash Occlusion

(c) Low Illumination Level (d) Eye Rotation

Figure 5: Segmentation Result

Table 1: Performance comparison

Methods	Segmentation Accuracy (%)	Recognition Accuracy	Image Quality
[2]	45	0.9832	0.9901
[6]	95	0.9701	0.9910
Proposed method	97	0.9729	0.9915

In terms of image quality, all methods achieved a high SSIM value. This showed that the Chan-Vese methods had less effect on image degradation compared to the other iris segmentation methods. The quality of iris pattern between the

original and processed iris images was not much different. Hence, the proposed method was efficient to be used in the real-time iris acquisition. The complete results are shown in Table 1.

4. CONCLUSION

This paper presents a modified Chan-Vese active contour for iris segmentation on non-ideal and noisy iris. In this study, the Chan-Vese active contour is modified by introducing a new equation to segment both non-ideal and noisy iris simultaneously. The proposed method is also developed to improve the segmentation accuracy, recognition accuracy and image quality of iris segmentation. Next, the proposed method is compared with the other Chan-Vese active contour iris segmentation methods. Two objectives are achieved: (a) segmenting non-ideal shape of pupillary and limbic boundaries in non-ideal iris; (b) segmenting iris region with the presence of noise in noisy iris. According to the results, the proposed method achieves the better performance than the other methods in terms of segmentation accuracy (97%), recognition accuracy (0.9729) and image quality (0.9915). These results show that the proposed method is efficient to overcome both non-ideal and noisy iris simultaneously.

ACKNOWLEDGEMENT

The authors gratefully acknowledge the Ministry of Higher Education Malaysia (MOHE) and the Universiti Teknologi MARA (UiTM) for making available the University Academic Training Scheme (SLAI).

REFERENCES

1. J. Daugman. **High confidence visual recognition of persons by a test of statistical independence**, *IEEE Transactions of Pattern Analysis and Machine Intelligent*, vol. 15, no. 11, pp. 1148–1161, 1993.
2. S. Jamaludin, N. Zainal, and W. M. D. W. Zaki. **Sub-iris technique for non-ideal iris recognition**, *Arabian Journal for Science and Engineering*, vol. 43, no. 12, pp. 7219–7228, 2018.
3. S. Jamaludin, N. Zainal, and W. M. D. W. Zaki. **The removal of specular reflection in noisy iris image**, *Journal of Telecommunication, Electronic and Computer Engineering*, vol. 8, no. 4, pp. 59–64, 2016.
4. S. Kadry, and K. Smaili. **A design and implementation of a wireless iris recognition attendance management system**, *Information Technology and Control*, vol. 36, no. 3, pp. 323–329, 2015.
5. S. Jamaludin, N. Zainal, and W. M. D. W. Zaki. **GPU implementation of sub-iris technique in iris recognition system**, *Pertanika Journal of Science and Technology*, vol. 25, no. S, pp. 263–274, 2017.
6. S. Jamaludin, N. Zainal, and W. M. D. W. Zaki. **Iris recognition based on the modified chan–vese active contour**, *Jurnal Teknologi*, vol. 78, no. 10–3, pp. 13–17, 2016.
7. S. Rapaka, and P. R. Kumar. **Efficient approach for non-ideal iris segmentation using improved particle swarm optimisation-based multilevel thresholding and geodesic active contours**, *IET Image Processing*, vol. 12, no. 10, pp. 1721–1729, 2018.
8. A. Radman, N. Zainal, and S. A. Suandi. **Automated segmentation of iris images acquired in an unconstrained environment using HOG-SVM and GrowCut**, *Digital Signal Processing*, vol. 64, pp. 60–70, 2017.
9. M. Kass, A. Witkin, and D. Terzopoulos. **Snakes: active contour models**, *International Journal of Computer Vision*, vol. 1, no. 4, pp. 321–331, 1988.
10. V. Caselles, R. Kimmel, and G. Sapiro. **Geodesic active contours**, *International Journal of Computer Vision*, vol. 22, no. 1, pp. 61–79, 1997.
11. T. F. Chan, and L. Vese. **Active contours without edges**, *IEEE Transactions on Image Processing*, vol. 10, no. 2, pp. 266–277, 2001.
12. P. Getreuer. **Chan-Vese segmentation**, *Image Processing On Line*, vol. 2, pp. 214–224, 2012.
13. Y. Yuan, and C. He. **Adaptive active contours without edges**, *Mathematical and Computer Modelling*, vol. 55, no. 5-6, pp. 1705–1721, 2012.
14. A. E. Rad, M. S. M. Rahim, H. Kolivand, and I. B. M. Amin. **Morphological region-based initial contour algorithm for level set methods in image segmentation**, *Multimedia Tools and Applications*, vol. 76, no. 2, pp. 2185–2201, 2017. https://doi.org/10.1007/s11042-015-3196-y
15. K. Ding, L. Xiao, and G. Weng. **Active contours driven by local pre-fitting energy for fast image segmentation**, *Pattern Recognition Letters*, vol. 104, pp. 29–36, 2018.
16. K. Ding, L. Xiao, and G. Weng. **Active contours driven by region-scalable fitting and optimized Laplacian of gaussian energy for image segmentation**, *Signal Processing*, vol. 134, pp. 224–233, 2017.
17. H. K. Rana, M. S. Azam, M. R. Akhtar, J. M. Quinn, and M. A. Moni. **A fast iris recognition system through optimum feature extraction**, *PeerJ Computer Science*, vol. 5, pp. e184, 2019.
18. A. A. Ghali, S. Jamel, K. M. Mohamad, N. A. Yakub, and M. M. Deris. **A review of iris recognition algorithms**, *JOIV: International Journal on Informatics Visualization*, vol. 1, no. 4-2, pp. 175–178, 2017.
19. N. Larbi, and N. Taleb. **A robust multi-biometric system with compact code for iris and face**, *International Journal on Electrical Engineering and Informatics*, vol. 10, no. 1, pp. 1–13, 2018.
20. N. Ahmadi, and M. Nilashi. **Iris texture recognition based on multilevel 2-d haar wavelet decomposition and hamming distance approach**, *Journal of Soft*

Computing and Decision Support Systems, vol. 5, no. 3, pp. 16–20, 2018.

21. A. Al-Qerem, and A. Alahmad. **Human body poses recognition using neural networks with data augmentation**, *International Journal of Advanced Trends in Computer Science and Engineering*, vol. 8, no. 5, pp. 2117–2120, 2019. https://doi.org/10.30534/ijatcse/2019/40852019
22. R. N. Butris, and H. M. Haji. **Periodic solutions for nonlinear systems of integro-differential equations of Volterra-Friedholm type**, *International Journal of Advanced Trends in Computer Science and Engineering*, vol. 8, no. 5, pp. 2078–2088, 2019. https://doi.org/10.30534/ijatcse/2019/35852019
23. A. Al-Qerem. **Circular shape formation using self adaptive collective motion of swarm robots**, *International Journal of Advanced Trends in Computer Science and Engineering*, vol. 8, no. 5, pp. 2054–2061, 2019. https://doi.org/10.30534/ijatcse/2019/32852019
24. S. Jamaludin, N. Zainal, and W. M. D. W. Zaki. **Comparison of iris recognition between active contour and hough transform**, *Journal of Telecommunication, Electronic and Computer Engineering*, vol. 8, no. 4, pp. 53–58, 2016.
25. A. Noruzi, M. Mahlouji, and A. Shahidinejad. **Iris recognition in unconstrained environment on graphic processing units with CUDA**. *Artificial Intelligence Review*, vol. 53, no. 5, pp.3705-3729, 2019.